Cell

Condensins Regulate Meiotic DNA Break Distribution, thus Crossover Frequency, by Controlling Chromosome Structure

David G. Mets[1,2,3] and Barbara J. Meyer[1,2,*]
[1]Howard Hughes Medical Institute
[2]Department of Molecular and Cell Biology
University of California, Berkeley, Berkeley, CA 94720-3204, USA
[3]Present address: Keck Center for Integrative Neuroscience, Department of Physiology, University of California, San Francisco, San Francisco, California 94143-0444, USA
*Correspondence: bjmeyer@berkeley.edu
DOI 10.1016/j.cell.2009.07.035

SUMMARY

Meiotic crossover (CO) recombination facilitates evolution and accurate chromosome segregation. CO distribution is tightly regulated: homolog pairs receive at least one CO, CO spacing is nonrandom, and COs occur preferentially in short genomic intervals called hotspots. We show that CO number and distribution are controlled on a chromosome-wide basis at the level of DNA double-strand break (DSB) formation by a condensin complex composed of subunits from two known condensins: the *C. elegans* dosage compensation complex and mitotic condensin II. Disruption of any subunit of the CO-controlling condensin dominantly changes DSB distribution, and thereby COs, and extends meiotic chromosome axes. These phenotypes are cosuppressed by disruption of a chromosome axis element. Our data implicate higher-order chromosome structure in the regulation of CO recombination, provide a model for the rapid evolution of CO hotspots, and show that reshuffling of interchangeable molecular parts can create independent machines with similar architectures but distinct biological functions.

INTRODUCTION

In sexually reproducing organisms, reassortment of gene combinations occurs through crossover (CO) recombination, the reciprocal exchange of DNA between homologous parental chromosomes. COs increase the genetic diversity upon which natural selection acts, thereby facilitating evolution. COs occur during meiosis, a specialized cell division that produces haploid sperm and eggs from diploid progenitor cells through two successive rounds of chromosome segregation that follow one round of DNA replication. COs are not randomly distributed along a chromosome but instead occur preferentially in short intervals called "hotspots" (Kauppi et al., 2004; Petes, 2001). In yeast, mice, and humans, recombination at hotspots occurs over intervals that range from 1 bp to 3 kb (de Massy et al., 1995; Jeffreys et al., 2001; Xu and Kleckner, 1995). Hotspots flank more evolutionarily stable regions known as haplotype blocks, which undergo recombination infrequently (Greenawalt et al., 2006; Kauppi et al., 2007). Mechanisms that dictate hotspot locations are poorly understood but of great interest, as hotspots determine the evolutionary landscape of the genome.

Studies have defined local factors that regulate CO hotspot activity, but no single model explains hotspot activity at all locations. A hotspot can be controlled by local DNA sequence, chromatin state, DNA methylation, or a combination of such factors (Kauppi et al., 2004; Maloisel and Rossignol, 1998; Petes, 2001). However, exclusively local regulation is in conflict with the evolutionary stability of hotspots (Boulton et al., 1997) and with the large, heritable, and rapid fluctuations in usage of multiple hotspots in human populations (Coop et al., 2008). Such fluctuations are difficult to achieve by simultaneous reassortment of DNA polymorphisms at multiple loci. However, a polymorphism in one locus that exerts genome-wide effects could cause rapid, simultaneous fluctuations. Our work identifies a protein complex in the nematode *C. elegans* that mediates rapid fluctuations in CO sites. Disruption of any subunit causes a dominant change in the genome-wide distribution of COs in a single generation.

CO hotspots correlate with hotspots for DNA double-strand breaks (DSBs), programmed events that initiate CO formation (Buhler et al., 2007; Gerton et al., 2000; Mancera et al., 2008). However, not all DSBs become COs. DSBs can be resolved instead as noncrossovers (NCOs) through repair without reciprocal DNA exchange using the homolog as a template. In yeast, approximately twice as many DSBs occur as COs; in mice, the ratio is more extreme, about ten to one (Buhler et al., 2007; Chen et al., 2008; Mancera et al., 2008; Moens et al., 2002). CO distribution can, in principle, be controlled through DSB placement or a bias in the CO/NCO decision imposed after DSB formation, but the relative contribution of each mechanism is unknown. The CO/NCO decision has been considered the predominant determinant in CO distribution.

Our work in *C. elegans* and recent work in yeast highlight the regulation of DSB placement in the control of CO distribution.

A genome-wide study of yeast recombination showed that identifiable DSB repair products (COs and NCOs) are farther apart than expected by chance (Mancera et al., 2008). Nonrandom positioning of COs and NCOs suggests that control of CO distribution might occur as early as DSB formation. We show that dramatic changes in DSB distribution in the nematode genome, under conditions that maintain or increase DSB number, correlate directly with changes in CO positions. Thus, CO regulation can occur at or before DSB formation.

COs undergo another form of regulation to ensure that each pair of homologous chromosomes has at least one CO, termed the obligate CO (Jones, 1984). This regulation is essential for chromosome segregation during meiosis, because a CO forms the physical link, or chiasma, between homologs (Page and Hawley, 2003). Without such linkage, aneuploid gametes occur. In many species, the number of COs per chromosome is low (Jones, 1984). *C. elegans* is an extreme case: only one CO occurs per homolog pair (Hillers and Villeneuve, 2003). Despite low CO frequency, chromosomes with no COs are extremely rare (Villeneuve, 1994). Our studies show that part of the mechanism to ensure an obligate CO occurs through DSB regulation.

When multiple COs occur on a given chromosome, COs are spaced farther apart than predicted by chance, a phenomenon known as CO interference (Sturtevant, 1913). Whether interference occurs at the level of DSB initiation or a more downstream step of CO regulation has not been fully assessed. Furthermore, the mechanistic relationship, if any, between CO interference and the obligate CO is not known.

Our work shows not only that COs can be controlled on a chromosome-wide basis through DSB initiation, but also that DSB position is strongly influenced by meiotic chromosome structure. Our previous work identified the *C. elegans* protein DPY-28, which regulates X chromosome dosage compensation (DC) in somatic cells and meiotic CO number and distribution in germ cells (Tsai et al., 2008). In the soma, DPY-28 acts in the dosage compensation complex (DCC), which resembles condensin, a conserved protein complex that mediates global chromosome restructuring to achieve accurate chromosome segregation (Losada and Hirano, 2005; Tsai et al., 2008). In this study, we show that DPY-28 controls CO distribution by functioning in a third condensin complex defined concurrently in our work and that of Csankovszki et al. (2009). This complex is distinct from the two known *C. elegans* condensins—the DCC and mitotic condensin II—but contains subunits from both. Disrupting any subunit of the CO-controlling condensin changes the distribution of DSBs, and thereby COs, and also increases CO frequency by increasing DSBs. Also, disruption of a condensin II-specific subunit changes CO disribution, but in different chromosomal domains. Condensin subunit disruption dominantly extends chromosome axes, implying that chromosome structure imposed by condensin controls meiotic CO recombination by regulating DSB formation.

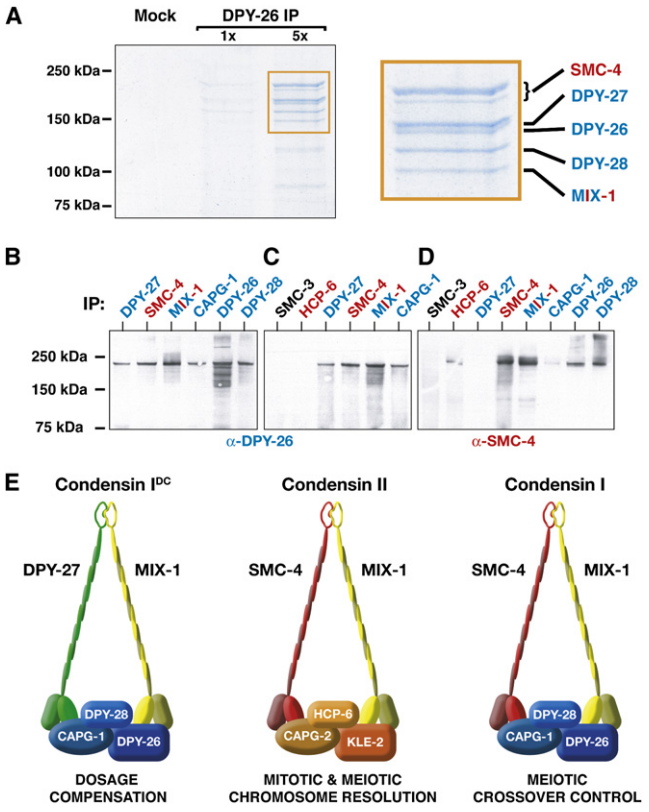

Figure 1. Identification of a Condensin Complex that Controls CO Distribution

(A) Colloidal blue stained proteins from SDS-PAGE-fractionated IP reactions using DPY-26 antibodies and protein extracts from mixed-stage worms. Proteins were identified by mass spectrometry (Table S1). Red, condensin II subunit; blue, condensin I^{DC} subunit; red-blue, subunit in both complexes.

(B–D) Reciprocal IPs and Western blot analysis using L4 extracts. The color scheme is as in (A).

(B) Reciprocal IPs confirm association of DPY-26 with condensin II subunit SMC-4, condensin I^{DC} subunits DPY-27, CAPG-1, and DPY-28, and subunit MIX-1, common to condensin II and condensin I^{DC}. Antibodies for IPs are above the blots and antibodies for probes below.

(C) IP for cohesin subunit SMC-3 (black) failed to recover DPY-26, showing that protein associations in (A) and (B) are not mediated by DNA. An IP for condensin II subunit HCP-6 failed to recover DPY-26, showing that DPY-26 does not associate with all condensin II subunits. DPY-27, SMC-4, MIX-1, and CAPG-1 IPs are positive controls.

(D) Reciprocal IPs verify the association of SMC-4 with condensin I^{DC} subunits CAPG-1, DPY-26, DPY-28 and with shared condensin subunit MIX-1. DPY-27 IPs identify DPY-26 but not SMC-4. HCP-6 IPs identify SMC-4 but not DPY-26, indicating that HCP-6 and DPY-27 are not part of condensin I.

(E) Subunit composition of three condensin complexes in *C. elegans*: condensin I^{DC}, condensin II, and condensin I. Condensin I, inferred from data in (A)–(D), includes the two SMC proteins MIX-1 and SMC-4 from mitotic condensin II and the three non-SMC proteins DPY-28, DPY-26, and CAPG-1 from condensin I^{DC}.

RESULTS

Biochemical Identification of a Condensin Complex with Subunits from Condensin I^{DC} and Condensin II

To identify proteins that act with DPY-28 to control COs, we conducted biochemical (Figure 1) and genetic (Figure 2) experiments. We asked whether null alleles of DC genes *dpy-26* and *dpy-27* alter CO distribution and found that *dpy-26* but not *dpy-27* mutations shift COs toward the right end of X and increase CO frequency due to double and triple COs, like *dpy-28* mutations (Figure 2A, and Figure S1A available online). Double COs were also higher on autosomes (Figure S1B).

A

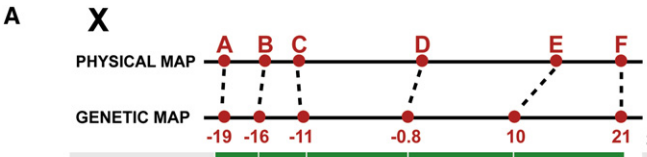

						3-CO	2-CO	1-CO	0-CO (%)	n
+/+	0.05	0.09	0.10	0.09	0.10	0	0	150	198 (57)	348
dpy-28(s939)/+	0.10	0.18	0.17	0.24*	0.22*	2	11*	57	24 (26)	94
dpy-28(y283)/+	0.00	0.00*	0.00*	0.18	0.33*	0	0	49	47 (49)	96
dpy-26(n199)/+	0.07	0.18	0.18	0.23*	0.22*	1	14*	51	26 (28)	92
mix-1(mn29)/+	0.11	0.12	0.09	0.23*	0.21*	4*	14*	27	50 (53)	95
smc-4(tm1860)/+	0.05	0.10	0.16	0.19*	0.12	0	7*	45	42 (45)	94
capg-1(tm1514)/+	0.05	0.13	0.17	0.18*	0.16	2	9*	126	60 (33)	183
dpy-27(y167)/+	0.04	0.11	0.16	0.10	0.12	0	1	39	41 (51)	81
dpy-27(y167)	0.03	0.07	0.08	0.08	0.09	0	0	31	61 (66)	92

B

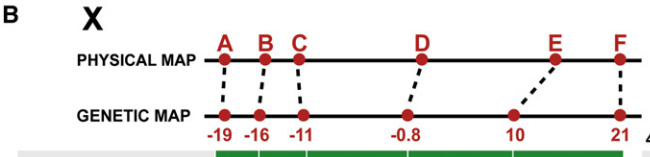

						4-CO	3-CO	2-CO	1-CO	0-CO (%)	n
+/+	0.05	0.09	0.10	0.09	0.10	0	0	0	150	198 (57)	348
+/+ (γ-Irradiated, 1.9 Gy)	0.11	0.09	0.08	0.03	0.06	0	0	0	32	62 (66)	94
+/+ (γ-Irradiated, 3.8 Gy)	0.04	0.14	0.12	0.10	0.11	0	0	4*	39	47 (52)	90
+/+ (γ-Irradiated, 7.5 Gy)	0.13	0.18	0.09	0.09	0.08	0	1	13*	24	57 (60)	95
dpy-28(s939)/+	0.10	0.18	0.17	0.24*	0.22*	0	2	11*	57	24 (26)	94
dpy-28(s939)/+ (7.5 Gy)	0.24*	0.15	0.30*	0.33*	0.30*	3*	10*	20*	35	17 (20)	85
dpy-26(n199)/+	0.07	0.18	0.18	0.23*	0.22*	0	1	14*	52	26 (28)	92
dpy-26(n199)/+ (7.5 Gy)	0.26*	0.12	0.26*	0.32*	0.25*	4*	12*	21*	22	26 (31)	85

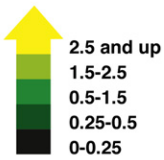

Relative Recombination Frequency (Mutant/Wild-Type)

Figure 2. Mutation of any Gene Encoding a Condensin I Subunit Increases CO Frequency and Shifts CO Distribution to the Right End of X

CO analysis of X in heterozygous condensin I mutants using snip-SNPs. The relative physical and genetic positions of SNPs (red) used to map CO sites are above the chart. For each genotype (left), the CO frequencies (numbers in the colored boxes) were calculated by the formula (number of COs in the interval)/(total meiotic products assayed). Box colors represent the relative recombination frequencies in each interval between mutant and wild-type animals; the key is at the bottom. Shown to the right are the number of triple (3-CO), double (2-CO), single (1-CO), and non- (0-CO) crossover chromatids and the total number (n) of chromatids scored. (%), Percentage of 0-COs was calculated by the formula 100(0-CO/n). Asterisks mark CO intervals or frequencies statistically different ($p < 0.01$, Fisher's exact test) from those in wild-type animals.

(A) Heterozygous mutations in condensin I genes shift COs to the right end of X, but mutation of DC-specific gene *dpy-27* does not. *dpy-28(y283)/+* data are from Tsai et al. (2008).

(B) γ-irradiation increases the number of COs on the left end of X and has an additive effect on CO frequency when combined with *dpy-28* or *dpy-26* mutations.

Immunoprecipitation (IP) reactions performed with DPY-26 antibodies and protein extracts from mixed-stage animals then defined additional proteins that control COs. IPs were fractionated by SDS-PAGE and proteins identified by mass spectrometry (Figure 1A, Table S1). As expected, the DPY-26 IP recovered subunits DPY-26, DPY-27, DPY-28 from the DCC condensin core (condensin I^{DC}), and MIX-1, a subunit shared by condensin I^{DC} and condensin II. Unexpectedly, the IP also recovered condensin II subunit SMC-4, suggesting that DPY-26 acts in a complex distinct from the DCC and that subunits of two different condensins act together in a third condensin complex.

Protein interactions were confirmed by reciprocal IPs and western blot analysis (Figures 1B–1D). In coIPs, SMC-4 antibodies recovered DPY-26, and antibodies to condensin I^{DC}

subunits DPY-26, DPY-28, and CAPG-1 recovered SMC-4, confirming the association of DC proteins with condensin II subunits. Although the DC protein CAPG-1 was not detected in the initial IP, it was detected in all subsequent IPs.

Controls verify the composition of this third condensin complex, named condensin I, which differs from condensin I^{DC} by substituting SMC-4 for DPY-27 (Figure 1E). Antibodies to the DC-specific SMC protein DPY-27 did not recover SMC-4 (Figure 1D). Antibodies to condensin II subunit HCP-6, a paralog of DPY-28, recovered SMC-4 but not DPY-26, showing that DPY-26 does not interact with all condensin II subunits (Figures 1C and 1D). Furthermore, neither DPY-26 nor SMC-4 was detected in IPs using antibodies to SMC-3, a subunit of cohesin, an SMC-containing complex that achieves chromosome cohesion and binds to chromosomes throughout meiosis. Thus, protein interactions identified by IPs are likely to be direct rather than mediated though DNA (Figures 1C and 1D).

Together, these results suggest that DPY-28 controls CO distribution through its action in a condensin complex distinct from condensin I^{DC} and condensin II, but composed of subunits from both (Figure 1E): the two SMC proteins MIX-1 and SMC-4 from mitotic condensin II (Hagstrom et al., 2002) and the three non-SMC proteins DPY-28, DPY-26, and CAPG-1 from condensin I^{DC} (Csankovszki et al., 2009; Meyer, 2005; Tsai et al., 2008). Concurrent studies also identified condensin I and showed it functions in mitosis (Csankovszki et al., 2009).

Condensin I Regulates Meiotic CO Number and Distribution

If all components of the biochemically defined condensin I complex act together in vivo to control COs, mutations that disrupt the function of any subunit should perturb COs similarly to *dpy-26* and *dpy-28* mutations. This premise held true. COs were assessed by examination of the segregation of snip-SNP markers, single-nucleotide polymorphisms (SNPs) that are restriction fragment length polymorphisms. Scoring snip-SNPs along individual chromosomes allowed us to monitor three aspects of CO recombination: CO frequency in a given interval, distribution of COs, and the number of COs on a single chromatid. Six snip-SNPs were used to assay a 40 cM interval corresponding to 80% of X. Since *dpy-28* mutations have a dominant effect on CO distribution (Tsai et al., 2008), comparison could be made using heterozygous mutations, thus averting complications from recessive lethality.

Animals heterozygous for a null allele of any gene encoding a condensin I subunit showed a striking shift in the CO distribution to the right side of X (Figures 2A and S1). The CO frequency was increased ~2- to 3-fold ($p < 0.005$, Fisher's exact test) in the D–F interval of *dpy-28*/+, *dpy-26*/+, *mix-1*/+, *smc-4*/+, and *capg-1*/+ mutants compared to that of wild-type animals. However, the CO pattern of animals heterozygous or homozygous for a null allele of DC gene *dpy-27* resembled that of wild-type animals, indicating that disruption of condensin I^{DC} does not shift the CO pattern. Thus, condensins that differ by only one subunit function in dramatically different chromosome-wide processes: dosage compensation and meiotic CO control.

In addition to altering CO distribution, condensin I disruption increased the number of double (2-CO) and triple (3-CO) crossovers (Figure 2A). Wild-type *C. elegans* exhibits tight control of meiotic COs. With rare exception, one CO occurs per homolog pair. In our experiments, wild-type animals had one CO per X homolog pair. In contrast, *dpy-26*/+ mutants had 14 2-COs and one 3-CO in 92 X homologs, while *mix-1*/+ mutants had 14 2-COs and four 3-COs in 95 X homologs ($p < 1 \times 10^{-5}$, Fisher's exact test). CO numbers resemble those of *dpy-28(s939)*/+ mutants, which had 11 2-COs and two 3-COs on 94 X homologs. In contrast, disruption of condensin I^{DC} did not alter CO number: *dpy-27*/+ and *dpy-27*/*dpy-27* mutants had wild-type CO levels (Figure 2A). These genetic experiments corroborate the conclusion from biochemical experiments that DPY-28 acts in a condensin complex made of subunits from two condensins: one that controls gene repression and one that controls chromosome segregation. Moreover, these experiments show that a condensin complex restricts meiotic CO number and distribution, a role previously unknown for condensins.

The Shift in CO Distribution Correlates Directly with the Shift in RAD-51 Foci in *dpy-28* Mutants

Depleting any condensin I subunit causes redistribution of COs, permitting us to ask whether the shift in CO position correlated with a change in DSB position. DSB distribution was compared along the length of X chromosomes in wild-type animals and mutants homozygous for the *dpy-28(y283)* partial loss-of-function allele, which dramatically shifts CO position without changing CO number (Figures 3 and 2A). DSBs were marked with an antibody to RAD-51, a RecA homolog that binds to nascent recombination intermediates just after DSB formation (Alpi et al., 2003; Ogawa et al., 1993). Meiotic chromosomes were labeled with antibodies to the axis marker HTP-3 and two fluorescence in situ hybridization (FISH) probes corresponding to the center and right end of X (Figure 3A). Positions of RAD-51 foci were scored relative to the FISH probes on chromosomes in which the axis (HTP-3) was traced in three dimensions (3D). Direct correlation between DSB and CO positions predicts a decrease in RAD-51 foci on the left end of X, where CO frequency is reduced and the genetic map compressed in mutants, and an increase in RAD-51 foci on the right end, where CO frequency is increased and the map expanded. The prediction was met.

In *dpy-28(y283)* mutants, COs decreased dramatically in the genetic interval A–D, and the percentage of total RAD-51 foci decreased correspondingly, from 44% in wild-type animals to 3% in *y283* mutants ($p < 1 \times 10^{-3}$, Fisher's exact test) (red interval, Figures 3B and 3C). In contrast, COs increased dramatically in the D–F interval, and the total RAD-51 foci increased from 50% to 80% ($p < 0.002$, Fisher's exact test) (blue interval, Figures 3B and 3C). The strong correlation between the locations of COs and RAD-51 foci in wild-type and mutant animals suggests that condensin I regulates COs by influencing DSB position. In broader perspective, mutation of a single gene can dramatically alter the landscape of CO hotspots along an entire chromosome, a phenomenon that suggests a model for rapid changes in hotspot usage.

A TUNEL Assay to Monitor DSBs

Consistent with a DSB increase causing the CO increase in condensin I mutants, we found that disrupting any condensin I

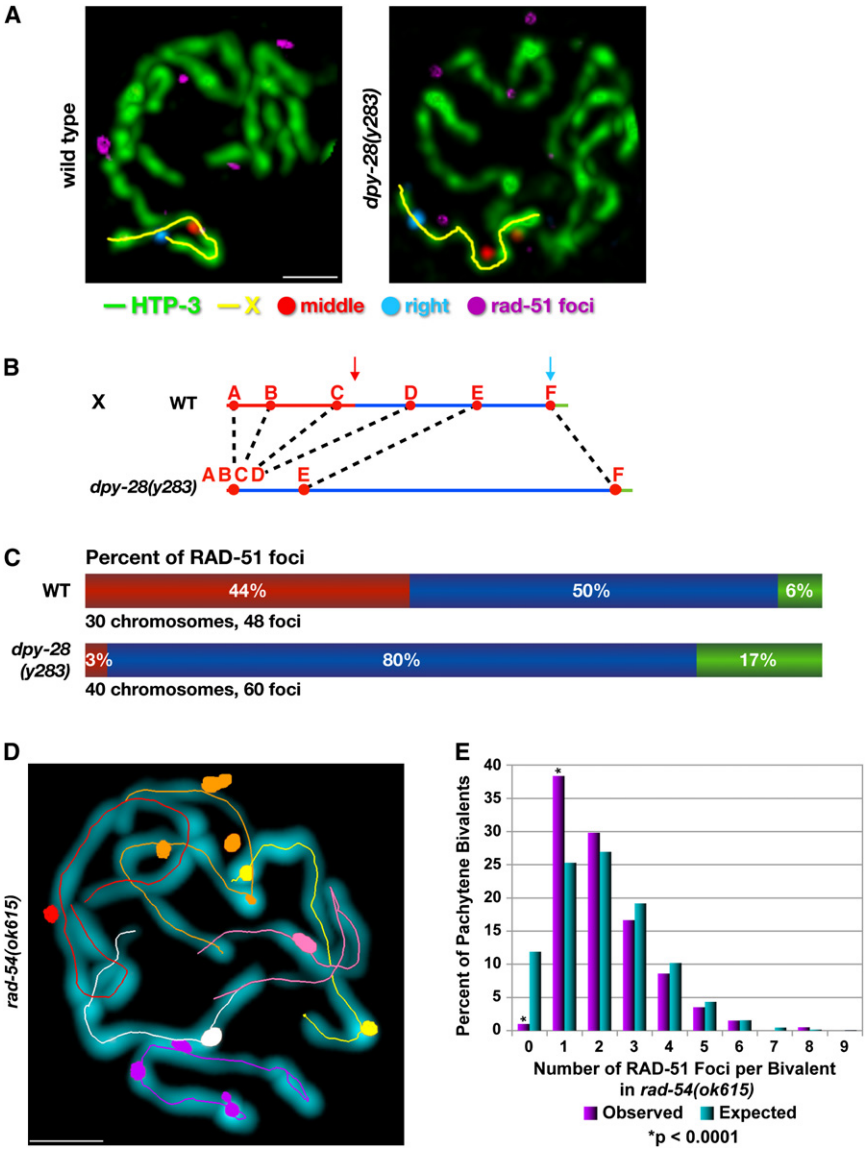

Figure 3. The Shift in CO Distribution Correlates Directly with the Shift in RAD-51 Distribution in *dpy-28(y283)* Mutants

(A) Pachytene chromosomes from wild-type and *dpy-28(y283)* animals labeled with X chromosome FISH probes from the center (red) and right end (blue) of X and antibodies to axial element HTP-3 (green) and RAD-51 (purple). X chromosome traces (yellow) are used to straighten each X and permit assessment of RAD-51 positions relative to FISH probes.

(B) The relative genetic maps of *dpy-28(y283)* and wild-type animals show that interval A-D is reduced in CO frequency in *y283* and interval D-F is increased. Individual SNPs scored are shown as red circles. Distances between SNPs reflect the frequency of COs between SNPs. Boundaries between red and blue intervals (red arrow) or blue and green intervals (blue arrow) are the approximate genetic positions of middle (red) or right-end (blue) FISH probes, respectively. *dpy-28(y283)* CO data are from Tsai et al. (2008).

(C) *dpy-28(y283)* mutants show a dramatic decrease in RAD-51 foci in the left interval (A–D, red) of X, which has map compression, and a dramatic increase in RAD-51 foci in the center interval (D-F, blue), which has map extension. Values shown in white are the percent of total RAD-51 foci in each interval (left, red; middle, blue; right, green) as demarcated by FISH probes. The number of X chromosomes and RAD-51 foci scored for each genotype are shown below each graph. The number of foci in red and blue intervals are statistically different between wild-type and *dpy-28(y283)* animals ($p < 0.002$, Fisher's exact test).

(D and E) An obligate DSB.

(D) Three-dimensional traces of chromosomes in a *rad-54(ok615)* pachytene nucleus (P2) permit quantification of RAD-51 foci per bivalent. Chromosomal axes are stained with HTP-3 antibodies (turquoise). Each chromosome trace is matched in color to its RAD-51 foci.

(E) An obligate DSB. Quantification of RAD-51 foci (purple) on each of 198 bivalents from 33 *rad-54(ok615)* pachytene (P2) nuclei is plotted relative to the expected number of foci (turquoise) in each category based on the Poisson distribution. The y axis shows percentage of bivalents having the number of RAD-51 foci given on the x axis. The number of bivalents with zero foci (1%) is significantly less than expected, and the number with one focus (38%) is significantly more ($p < 0.0001$, binomial test), revealing a mechanism to guarantee at least one DSB per bivalent.

Scale bars represent 1 μm.

subunit, but not condensin I^{DC} subunit DPY-27, increased RAD-51 foci (see below, and Figures S2 and S5L). However, three models can explain this increase: condensin I disruption could increase the total number of DSBs, slow the repair of DSBs, or increase the proportion of DSBs being repaired through RAD-51 intermediates. The latter model is unlikely, as repair pathways not involving RAD-51 are rarely utilized in *C. elegans* meiosis (Martin et al., 2005). We combined two new approaches to distinguish between the other two models and found an increase in DSBs: (1) We developed an independent assay, the TUNEL assay, to monitor DSBs directly (Figure 4), and (2) we found mutant conditions (*rad-54*) that block DSB repair and hence trap DSBs and DSB-bound RAD-51 proteins.

In the TUNEL assay, terminal deoxynucleotidyl transferase attached fluorescently labeled nucleotides to exposed 3′ ends of DSBs. Assay specificity was shown by the absence of foci in *spo-11* mutants, which lack the DSB-forming type II topoisomerase (Figures 4A and 4B) (Dernburg et al., 1998; Keeney et al., 1997). Quantification showed good agreement between TUNEL and RAD-51 foci in singly labeled germlines (Figures 4D and 4E). Throughout pachytene, levels of TUNEL and RAD-51 foci were similar. As expected, more TUNEL than RAD-51 foci were found in two germline regions: the premeiotic region, where DNA nicks occur during replication, and the transition zone (leptotene/zygotene) (Figure 4D), where the onset of DSB formation precedes RAD-51 binding (Padmore et al., 1991).

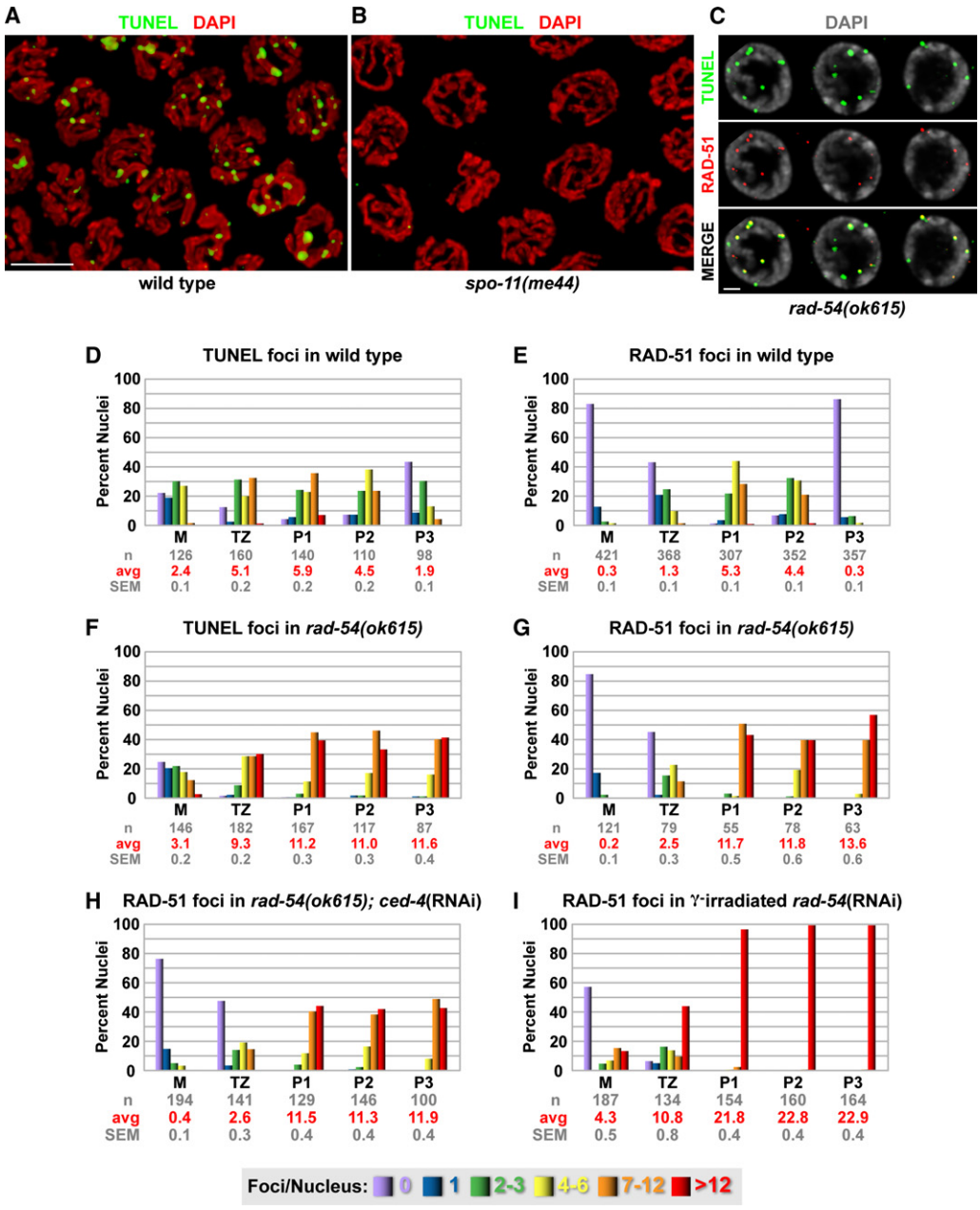

Figure 4. TUNEL Assay Shows that Twice as Many DSBs Occur as COs in *C. elegans*

(A and B) TUNEL assay detects SPO-11-dependent DSBs (green) on pachytene chromosomes (red). The scale bar represents 4 μm.

(C) Most TUNEL foci (green) colocalize with RAD-51 foci (red) in pachytene. The scale bar represents 1 μm.

(D–I) Histograms show quantification of either RAD-51 or TUNEL foci in wild-type or *rad-54(ok615)* germlines. Each column color represents a class of nuclei with the indicated number of foci. A color key is at the bottom. The y axis shows the percentage of foci in each class. The x -axis shows the position along the germline: premeiotic region (M), transition zone (TZ), the first third of pachytene (P1), the second third of pachytene (P2), and the last third of pachytene (P3). The number of nuclei (n) scored, the average number of foci (avg), and standard error of the mean (SEM) are shown beneath each stage.

(D and E) DSB number, as measured by TUNEL, correlates well with RAD-51 foci in wild-type germlines.

(F and G) The plateau value of DSBs and RAD-51 foci in pachytene nuclei of *rad-54(ok615)* germlines shows an average value of ~12 DSBs in each meiocyte, twice as many DSBs as COs.

(H) Elimination of germline cell death by *ced-4*(RNAi) in the *rad-54(ok615)* mutants reduces the average number of RAD-51 foci only in P3, where apoptosis occurs.

(I) γ-irradiation (7.5 Gy) of *rad-54*(RNAi) animals increases the plateau value of RAD-51 foci, indicating that RAD-51 and the machinery to make RAD-51 foci are not limiting in the *rad-54*(RNAi) animals.

Comparison of TUNEL and RAD-51 foci in colabeled germlines showed that nearly all RAD-51 foci corresponded to TUNEL foci (Figures 4C, S4E, S5A, S5C, and S5F–S5H). However, only 60%–70% of TUNEL foci colocalized with RAD-51 foci, because conditions for optimal TUNEL signal are not optimal for RAD-51 signal, as shown by comparison of RAD-51 and TUNEL foci quantified from singly labeled germlines versus colabeled germlines (Figures S5A–S5D, S5I, and S5J). Combined, our results show that TUNEL and RAD-51 foci in singly labeled germlines are excellent markers for DSBs in pachytene nuclei.

RAD-54 Depletion Traps All DSBs

In *S. cerevisiae*, *rad54* mutations disrupt the repair of DSBs and slow the removal of Rad51 (Shinohara et al., 2000). We found that in *C. elegans rad-54* mutants, DSBs and RAD-51 foci persist (Figures 4F, 4G, 5C, 5E, S3, and S4B) and remain colocalized (Figures 4C, S5C, and S5F). Furthermore, no DSBs occur in *rad-54; spo-11* double mutants, indicating that all DSBs are initiated by SPO-11 (Figure S3). Since DSBs are not repaired and RAD-51 foci not removed in *rad-54* mutants, the plateau value of TUNEL or RAD-51 foci should represent all DSBs repaired through a RAD-51 intermediate.

The average plateau value for DSBs and RAD-51 foci is 11–12 per nucleus in *rad-54* mutants (Figures 4F, 4G, 5C, and 5E). Since *C. elegans* has six pairs of homologs, only half the DSBs formed become COs. The implications will be addressed later.

Two controls further validate the use of *rad-54* mutants in DSB analysis. First, elimination of germline apoptosis in *rad-54(ok615)* mutants by RNA interference (RNAi) against the cell death gene *ced-4* showed that apoptosis does not significantly distort our overall estimate of RAD-51 foci, and measurements through mid-pachytene (P2) seem unaffected by cell death (Figures 4G and 4H). Second, extra DSBs induced in *rad-54*-deficient animals through γ-irradiation raised the average RAD-51 plateau value to ~23 foci, thus tempering any concern that the ~12 RAD-51 foci in *rad-54* mutants is an underestimate due to limiting RAD-51 protein or the machinery to produce RAD-51 foci (Figures 4I and S3, and controls in Figures 5C, 5E, and 5I).

Condensin I Regulates DSB Number

We found an average of 15.3 TUNEL and 14.3 RAD-51 foci in mid pachytene (P2) of *dpy-28(s939* null*); rad-54*(RNAi) mutants, compared to 12.1 TUNEL and 11 RAD-51 foci in *rad-54*(RNAi) animals (Figures 5B–5E, 5H, S3, and S4A–S4D). The degree of TUNEL and RAD-51 colocalization in *dpy-28(s939* null*); rad-54* (RNAi) double mutants or in *dpy-28(s939)* single mutants was the same as in *rad-54*(RNAi) or wild-type animals, respectively (Figures S4E, S5A, and S5F–S5H). Thus, the increase in RAD-51 foci in condensin-I-defective mutants (Figure 5A) is caused by an increase in DSB production, not a delay in DSB repair. Furthermore, the increase in CO number and occurrence of 2-COs and 3-COs in *dpy-28* null mutants correlates directly with the increase in DSB number. Thus, an important function of condensin I is to limit DSB number, and thereby limit CO number, and to regulate DSB distribution. Consistent with this conclusion, the *dpy-28(y283)* hypomorphic mutation caused redistribution of RAD-51 foci concomitantly with that of COs but increased neither RAD-51 foci nor COs (Figures 3A, 3B, 5E–5G, and 5I) (Tsai et al., 2008).

An Obligate DSB: An Active Mechanism Must Ensure One DSB per Homolog Pair

A pair of homologs (a bivalent) must have at least one CO to segregate properly in meiosis I (Page and Hawley, 2003). A mechanism that ensures an obligate CO could act by forming excess DSBs on each chromosome or by preventing random DSB distribution and thereby guaranteeing one DSB per bivalent. To assess the mechanism in *C. elegans,* we counted DSBs on bivalents. RAD-51 foci were counted on each of 198 pachytene bivalents from *rad-54(ok615)* gonads labeled for the axis marker HTP-3, imaged, and traced in 3D. The 3D tracing permits unambiguous assignment of each focus to one chromosome (Figure 3D). Given our average observed value of 2.1 RAD-51 foci per bivalent, the Poisson distribution predicts that a surprisingly large number of bivalents would lack a DSB to produce the obligate CO if DSB distribution were random. However, the distribution of RAD-51 foci does not fit the Poisson distribution (Figure 3E).

The number of bivalents with no RAD-51 foci was far lower than predicted, and the number with one focus far greater: only 1% of bivalents had zero RAD-51 foci compared to 12% expected, and 38% of bivalents had one focus compared to 25% expected (both, $p < 1 \times 10^{-4}$, binomial test) (Figure 3E). A large fraction of bivalents had only one DSB, which must form the obligate CO. Given that almost all chromosomes have one or more DSBs, while no chromosomes have more than one CO, two conclusions emerge. An active mechanism prevents random DSB distribution, thereby ensuring at least one DSB per bivalent. Such a process accounts, at least in part, for the mechanism that ensures an obligate CO. In addition, since 61% of chromosomes have two to six RAD-51 foci, some CO regulation must also occur after DSB formation, during the CO-NCO decision (Figure 3E). Thus, CO regulation in *C. elegans* occurs at two different levels.

Irradiated Animals Have an Increased CO Frequency but a CO Distribution Different from Condensin-I-Defective Mutants

Our findings that (1) CO regulation can occur at the level of DSB production and (2) condensin I disruption increases CO frequency by increasing DSB number predict that induction of extra DSBs by γ-irradiation should increase CO frequency. This expectation was met (Figure 2B). Successively higher doses of γ-irradiation caused a dose-dependent increase in CO frequency to a level comparable to that in *dpy-28(s939)* mutants (Figures 2A and 2B). However, the DSB number was 2-fold higher (~23 versus ~12 DSBs) in γ-irradiated animals, indicating that a higher proportion of DSBs became COs in condensin-I-defective mutants than in γ-irradiated animals. Although the overall CO frequency increased in γ-irradiated animals, the percentage of noncrossover chromatids did not change, unlike in mutants, which had a reduced percentage. γ-irradiation increased COs on the left end of X, while disruption of condensin I shifted COs to the right end (Figures 2A and 2B). Two

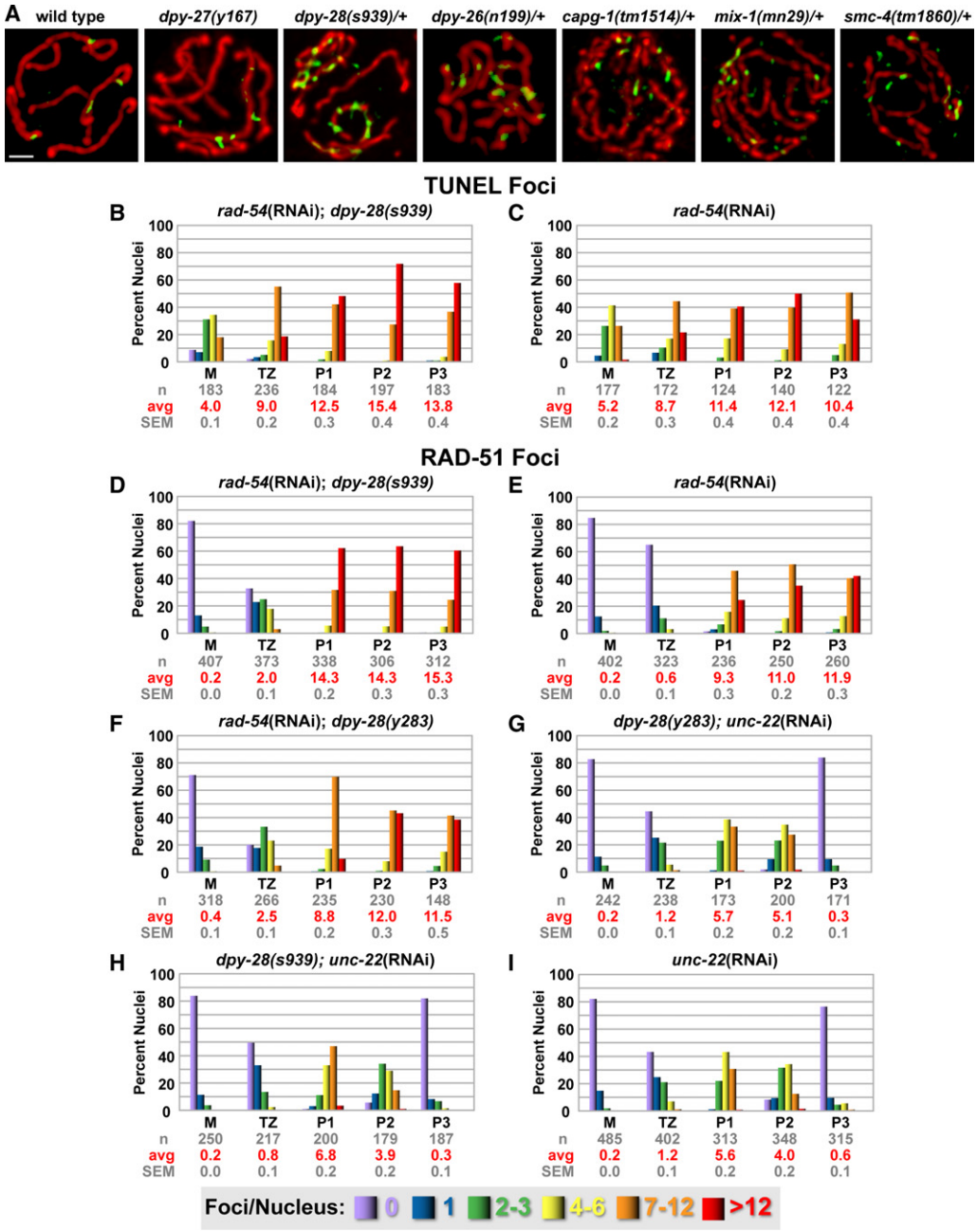

Figure 5. Condensin I Mutants Have More DSBs than Wild-Type Animals

(A) Shown are high-resolution images of early- to mid-pachytene nuclei from wild-type and mutant animals labeled with antibodies to RAD-51 (green) and the axis protein HTP-3 (red). Pachytene nuclei from mutants defective in the DCC-specific gene *dpy-27* have a similar number of RAD-51 foci as wild-type animals, while animals heterozygous for a mutation disrupting any condensin I subunit show an increase in RAD-51 foci. Fields of nuclei are shown in Figure S2. The scale bar represents 1 μm.

(B and C) Histograms show quantification of TUNEL foci in *rad-54*(RNAi); *dpy-28(s939)* or *rad-54*(RNAi) germlines. Histograms are labeled as in Figure 4. *rad-54*(RNAi); *dpy-28(s939)* mutants have a higher plateau value of TUNEL foci than *rad-54*(RNAi) animals (~15.4 versus ~12), consistent with the increase in COs and RAD-51 foci in the mutants. The average number of DSBs per nucleus in P1–P3 is statistically different between (B) and (C) ($p < 0.001$, two-tailed t test).

(D–I) Histograms show quantification of RAD-51 foci in mutant germlines, as labeled above.

(D and E) The average number of RAD-51 foci per nucleus in P1-P3 of *rad-54*(RNAi); *dpy-28(s939)* germlines (~14) is statistically different from that in *rad-54(ok615)* (Figure 4G) or *rad-54*(RNAi) germlines (~11) ($p < 0.001$, two-tailed t test), consistent with the s939-induced increase in COs.

(F and G) The plateau value of RAD-51 foci is similar in *rad-54*(RNAi); *dpy-28(y283)* and *rad-54*(RNAi) germlines, consistent with y283 not increasing COs.

(H and I) *dpy-28(s939); unc-22*(RNAi) germlines have increased RAD-51 foci compared to *unc-22*(RNAi) controls, which show the RNAi process does not affect RAD-51 foci (compare to Figure 4E).

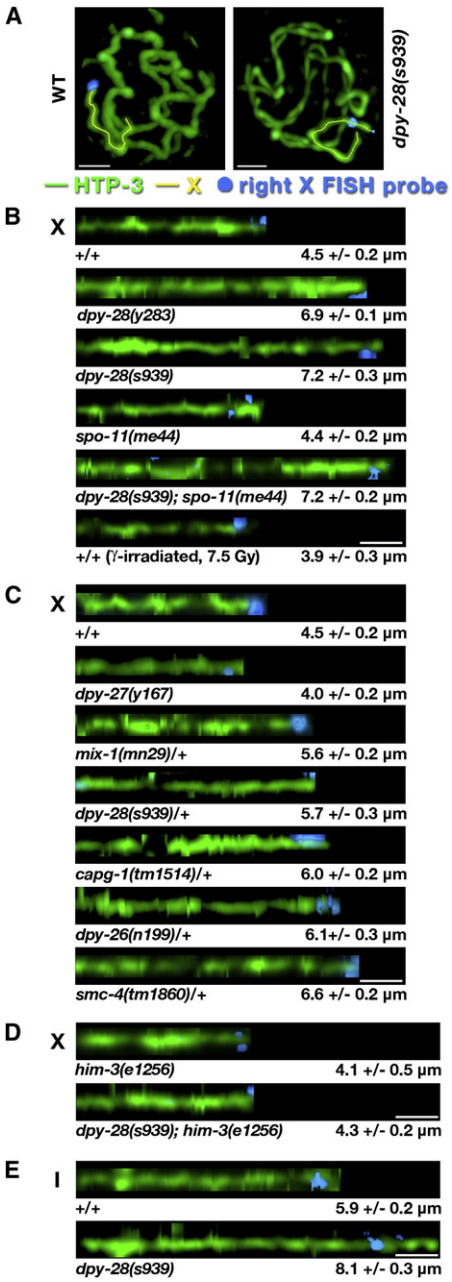

Figure 6. Meiotic Chromosome Axis Length Is Expanded in Condensin I Mutants

(A) Shown are high-resolution images of nuclei from the first third of pachytene in wild-type and *dpy-28(s939)* germlines labeled for the axis protein HTP-3 (green) and a right-end X FISH probe (blue). A 3D X chromosome trace (yellow) was used to straighten each chromosome.

(B–E) Computationally straightened chromosomes are displayed horizontally. Genotypes, average total axis length, and SEM are shown below each axis.

(B) Disruption of *dpy-28* causes an increase in X chromosome axis length that is independent of programmed DSBs made by SPO-11. Induction of extra DSBs by γ-irradiation does not increase axis length.

(C) Mutation of any gene encoding a condensin I subunit causes a haploinsufficient extension of x axis length. In contrast, mutation of the condensin I^{DC}-specific *dpy-27* gene does not.

(D) The axis expansion caused by disrupting condensin I requires axis protein HIM-3.

(E) The chromosome I axis is expanded in *dpy-28(s939)* mutants compared to wild-type animals. The scale bar represents 1 µm.

conclusions emerge. Increasing DSB number by two different agents has an additive effect on CO frequency. The difference in CO distribution caused by the two agents suggests the underlying mechanisms differ.

Involvement of two mechanisms predicts that γ-irradiation of *dpy-26* or *dpy-28* mutants should increase COs in an additive manner, an expectation met by our experiments (Figure 2B). The X chromosome genetic maps of γ-irradiated *dpy-28(s939)* or *dpy-26(n199)* mutants differ from the wild-type map in two ways: map expansion was observed in both the left (a hallmark of γ-irradiation) and the right (a hallmark of *dpy-26* and *dpy-28* mutants) ends of X. Furthermore, the number of chromatids with multiple COs was nearly additive. Our combined results show that condensin I disruption changes DSB distribution differently from γ-irradiation and that more DSBs are resolved into NCOs in irradiated animals. Both conditions reinforce the view that CO regulation can occur at the level of DSB production.

Disruption of Any Condensin I Subunit Expands the Axis of Meiotic Chromosomes

The role of condensin in controlling higher-order chromosome structure (Losada and Hirano, 2005) suggests the hypothesis that condensin I disruption might alter DSB position and frequency by altering chromosome structure, an effect not expected from γ-irradiation. Since a change in chromosome structure might alter axis length, we measured axis lengths of X and autosomes during CO formation in wild-type, mutant, and γ-irradiated animals (Figures 6A–6E and S6). The axis is the proteinaceous core of meiotic chromosomes around which DNA is organized into lampbrush-like structures (Page and Hawley, 2004).

We found that disruption of any condensin I subunit dramatically increased axis lengths of pachytene chromosomes (Figures 6 and S6). During all stages of pachytene, the *dpy-28(s939)* X axis was longer than the wild-type X axis (Figures 6B and S6). In early pachytene (P1), the mutant axis was extended by 1.6-fold (changed from 4.5 ± 0.2 µm to 7.2 ± 0.3 µm), and in late pachytene (P3) by 1.3-fold (changed from 5.7 ± 0.2 µm to 7.6 ± 0.2 µm) (Figure S6), consistent with a corresponding change in DSB and CO number and distribution. Similarly, the chromosome I axis was extended 1.4-fold in P1 of *dpy-28(s939)* mutants (changed from 5.9 ± 0.2 µm to 8.1 ± 0.3 µm) (Figure 6E).

The X axis extension in *dpy-28(s939)* mutants is independent of DSB production. Animals mutant for the meiotic DSB-forming enzyme *spo-11* had an X axis length (4.4 ± 0.2 µm) similar to that of wild-type animals, while *dpy-28(s939); spo-11* double mutants had an axis length (7.2 ± 0.2 µm) identical to that of *dpy-28(s939)* mutants (Figure 6B). The X axis length (3.9 ± 0.3 µm) of γ-irradiated animals was similar to that of wild-type animals. Thus, inducing more DSBs does not increase X axis length (Figure 6B). These data rule out the possibility that axis structure, as measured by length, is dictated by DSB formation and suggest

that the converse is true: axis structure regulates DSB position and frequency within the genome.

Disruption of any condensin I subunit extends X axis length, consistent with a change in CO number and distribution (Figure 6C). Axis extension ranged from 1.2- to 1.5-fold (5.6 ± 0.2 μm to 6.6 ± 0.2 μm) in heterozygous mutants versus wild-type animals, a significant change ($p < 1 \times 10^{-4}$, two-tailed t test) that was typically greater in homozygotes. For example, the X axis of *dpy-28(s939)*/+ heterozygotes was extended by 1.3-fold compared to 1.6-fold for *dpy-28(s939)* homozygotes (Figures 6B and 6C). In stark contrast, disruption of condensin I^{DC} failed to increase X axis length, which is shorter in *dpy-27* homozygotes (4.0 ± 0.2 μm) than in wild-type animals (Figure 6C). Thus, condensin I controls chromosome structure in early meiosis. Because axis proteins are loaded in yeast before DSBs form (Padmore et al., 1991) and the axial element HTP-3 is required in *C. elegans* for DSB formation (Goodyer et al., 2008), it is likely that changes in axis length due to condensin I disruption contribute directly to changes in DSB frequency and position.

Both Axis Expansion and DSB Increase in Condensin I Mutants Require Axis Protein HIM-3

Although the axis-associated protein HIM-3, a *C. elegans* homolog of the yeast axis protein Hop1, is not essential for DSB formation or repair in otherwise wild-type animals (Couteau et al., 2004), it is critical for the increase in RAD-51 foci in *dpy-28* mutants (Tsai et al., 2008). The number of RAD-51 foci and their kinetics of appearance and disappearance are very similar in *him-3*(null) single and *dpy-28(s939)*; *him-3*(null) double mutants. Thus, we asked whether a *him-3* mutation also suppresses axis expansion in *dpy-28* mutants. Suppression would strengthen the view that condensin I controls CO distribution by modulating chromosome structure. Homolog synapsis fails in *him-3*(null) mutants, making axes difficult to trace, so we examined axis length in *him-3(e1256)* missense, partial-loss-of-function mutants in which homolog synapsis is normal. We found that *dpy-28 (s939); him-3(e1256)* double mutants behave like *him-3(e1256)* single mutants with regard to the number and kinetics of RAD-51 foci (Figures S7A–S7D). Moreover, *him-3(e1256)* suppresses the axis expansion of condensin I mutants. Axis length in *dpy-28(s939); him-3(e1256)* double mutants (4.3 ± 0.2 μm) is similar to that in *him-3(e1256)* (4.1 ± 0.5 μm) and wild-type (4.5 ± 0.2 μm) animals, reinforcing the view that axis expansion influences DSB number and distribution (Figures 6B and 6D).

Disruption of Condensin II, like that of Condensin I, Expands Chromosomal Axes but Alters CO Distribution Differentially

The link between axis expansion and CO redistribution in condensin I mutants led us to ask whether disruption of condensin II also perturbs chromosome axes and alters CO distribution. Condensin II is required in *C. elegans* for restructuring meiotic chromosomes after pachytene exit to create compact diakinesis bivalents (Chan et al., 2004). Its roles in early meiosis have not been explored. Both condensin I and condensin II subunits, but not condensin I^{DC} subunit DPY-27, are enriched in premeiotic, transition zone, and pachytene nuclei and partially colocalize with DNA (Figures S8A–S8C). We found that condensin II affects CO distribution and axis length independently of condensin I. X axis length in *kle-2*(null)/+ condensin II mutants (5.8 ± 0.3 μm) is comparable to that in *dpy-28*(null)/+ condensin I mutants (5.7 ± 0.3 μm) (Figures 7A and 7B). However, the effects on axis length by the two condensins appear to be independent, because *dpy-28*/+; *kle-2*/+ double mutants have a longer X axis (8.0 ± 0.2 μm) than either single mutant, while animals with two condensin I mutations (genotype: *dpy-28*/+; *dpy-26*/+) have the same axis length as animals with one. Furthermore, the axis in *dpy-28*/+; *kle-2*/+ mutants is longer than in *dpy-28*/*dpy-28* mutants (7.2 ± 0.3 μm).

The axis expansion in *kle-2*/+ mutants is accompanied by an increase in DSBs (Figures 7C and S2), an increase in 2-COs, and a shift in CO distribution to the left end of X (Figure 7D), the opposite end of condensin I mutants, consistent with the two complexes acting independently. Thus, two distinct condensins affect CO distribution in different ways, but disruption of either complex causes an increase in COs correlated with expansion of chromosomal axes, strengthening the view that axis structure helps control COs.

DISCUSSION

A Role for Condensin in CO Regulation

Regulation of CO distribution was thought to occur after DSB formation, by directing a DSB to become a CO or NCO. We show that condensin controls CO distribution on a genome-wide basis via DSB formation. Higher eukaryotes have two condensin complexes (condensin I and II), which share two SMC subunits but have three distinct non-SMC subunits (reviewed in Losada and Hirano, 2005). The complexes play complementary but independent roles in restructuring chromosomes to achieve accurate segregation (Ono et al., 2003). In *C. elegans*, condensin II retains these critical functions, but prior to our work and the concurrent work of Csankovszki et al. (2009), the only known role for a condensin-I-like complex was in X chromosome repression during dosage compensation (Chan et al., 2004; Hagstrom et al., 2002; Meyer, 2005). *C. elegans* could have adapted condensin I for a new role and lost the old one, but we found that not to be the case. Our work revealed a third condensin, the bona fide condensin I. This new condensin is composed of subunits from condensin I^{DC} and condensin II but differs from condensin I^{DC} by only one subunit. *C. elegans* condensin I regulates DSB distribution, and thereby CO distribution, by controlling meiotic chromosome structure, a role not previously described for any condensin. Condensin I also functions in mitosis, but with less of a contribution than condensin II (Csankovszki et al., 2009; Tsai et al., 2008). Thus, reshuffling of interchangeable molecular parts creates independent machines with similar architectures but distinct functions.

An Obligate DSB

To achieve an obligate CO, at least one DSB must occur per homolog pair (bivalent). Two mechanisms could guarantee one DSB. Numerous DSBs might be formed randomly, yielding

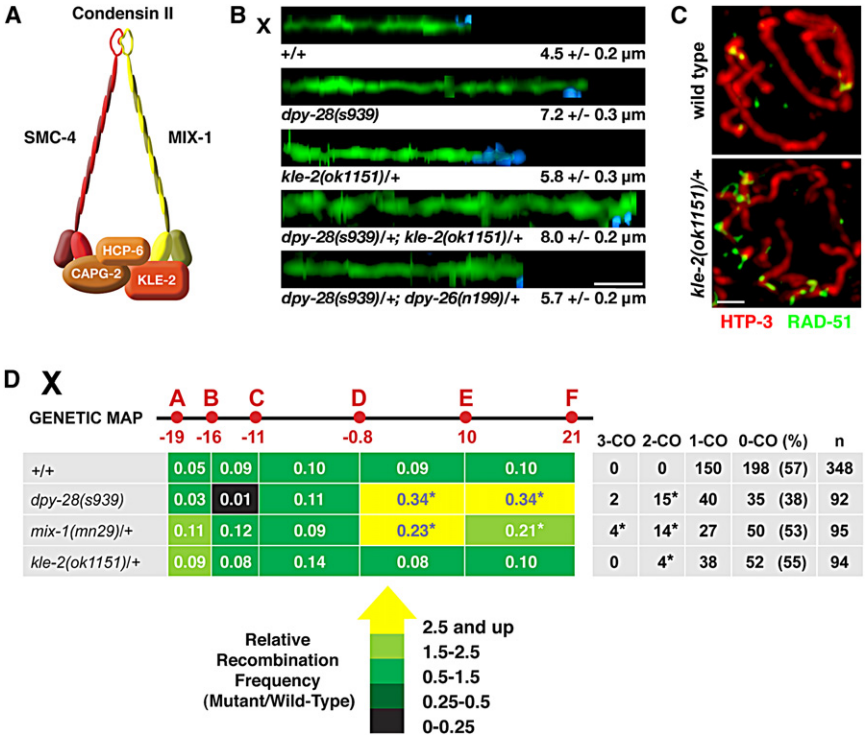

Figure 7. Condensin II Disruption Expands Chromosomal Axes but Alters CO Distribution Differently from Condensin I Disruption

(A) Condensin II complex.

(B) Straightened X chromosomes from pachytene nuclei. Genotypes, average axis length, and SEM are below each axis. X axis lengths in *kle-2* (null)/+ and *dpy-28*(null)/+ mutants are similar but longer than in wild-type animals. Axis length in *dpy-28*/+; *kle-2*/+ double mutants is greater than in either single mutant, but axis length in *dpy-28*/+; *dpy-26*/+ double mutants is similar to that in either single mutant, showing independent action of condensin II and I.

(C) Axis expansion in *kle-2*/+ pachytene chromosomes correlates with a DSB increase.

(D) *kle-2*/+ mutants show an increase in 2-COs and a shift in CO distribution to the left end of X, the opposite end of condensin I mutants. CO analysis and presentation are as in Figure 2. Asterisks mark CO intervals or frequencies statistically different ($p < 0.01$, Fisher's exact test) from those in wild-type animals. The scale bar represents 1 µm.

a high probability that each bivalent receives at least one. Alternatively, an active distribution mechanism might ensure that each bivalent receives a DSB, critical if total DSB number is low. Budding yeast and mice are thought to have ~10 times more DSBs than bivalents (Buhler et al., 2007; Moens et al., 2002), observations that are consistent with the first model but do not eliminate the second. The low ratio of DSBs to bivalents (2:1) we found in *C. elegans* provided a unique opportunity to test the models. Given an average of 2.1 DSBs per bivalent, random placement of DSBs predicted by the first model would lead to many bivalents with no DSBs. Contrary to this, we found almost no bivalents without a DSB, suggesting the second model is true. Furthermore, ~38% of bivalents had only one DSB, requiring it to be resolved as a CO. Thus, the *C. elegans* mechanism to ensure an obligate CO functions, at least in part, by an active process to ensure one DSB per bivalent. Moreover, since 61% of bivalents had two to six DSBs but one CO, COs must also be regulated at a later step, the CO/NCO decision.

Condensin and the Evolutionary Stability of Hotspots

The persistence of CO hotspots in a population is a paradox (Boulton et al., 1997). In yeast, mice, and humans, heterozygous hotspots specified by local DNA sequences are preferentially converted to the cold allele on the homolog via gene conversion, the nonreciprocal transfer of short DNA stretches during DSB repair (Jeffreys and Neumann, 2002; Nicolas et al., 1989; Yauk et al., 2003). The cause is an intrinsic bias for the hotspot allele to receive a DSB. Over time, these hotspots are culled from the genome. Paradoxically, many human hotspots are so active that gene conversion should have removed them, yet they persist (Coop and Myers, 2007). Their persistence is inconsistent with exclusively local control of CO activity. Coop and Myers (2007) suggested that nascent hotspots might undergo a period of inactivity during which they are refractory to transmission bias, thus allowing them to reach equilibrium and thereby slow their rate of loss.

Such a mechanism would be feasible if changes that activate hotspots occurred at distant sites. Our work provides a model: a single locus controls hotspot activity at multiple locations. Specifically, genome-wide changes in hotspot usage result from a polymorphism in any of several loci (condensin genes) that influence chromosome structure. Either chromosome-wide CO control could occur completely independently of local sequence, or broad genomic regions could be targeted for DSBs, after which local factors influence the choice of DSB site. In the latter model, a nascent hotspot could be sequestered from the DSB machinery for several generations until, for example, a change in chromosome structure caused by mutation of a condensin gene permitted its use for COs. Given that many hotspots have some local regulation, we favor the second model.

Genome-wide regulation of COs by *trans*-acting factors lends insight into two examples of rapid hotspot evolution. First, humans and chimpanzees share few, if any, CO hotspots despite having >97% DNA sequence identity, suggesting that hotspot usage evolves more rapidly than DNA sequence (Winckler et al., 2005). Second, hotspot usage changes rapidly among descendants in a human Hutterite population (Coop et al., 2008). Such diversity would be easy to achieve if a few factors, like condensin, regulate hotspot distribution across the genome in a concentration-dependent manner, but difficult to achieve by simultaneous reassortment of polymorphisms at multiple loci

over a few generations. The mouse Dsbc1 locus also shows that one locus (6.7 Mb) can affect CO distribution in many regions on different chromosomes, potentially contributing to rapid hotspot evolution (Grey et al., 2009).

Chromosome Structure: A CO Control Point

Our results show that an increase in axis length caused by depletion of any condensin subunit correlates with a dominant change in DSB distribution and CO position. Because DSB number does not influence axis length in our experiments and axis proteins load before DSBs are formed (Padmore et al., 1991; Goodyer et al., 2008), the axis expansion likely causes the change in DSB distribution. By extension, chromosome structure imposed by condensin controls CO position and frequency in wild-type animals by controlling DSB distribution. This view is enhanced by our finding that axis protein HIM-3 is required for both the DSB increase and the axis expansion in *dpy-28* mutants. Moreover, two different condensins, both I and II, affect DSB and CO distribution, but in different chromosomal domains. Disruption of both complexes expands axes more than disruption of either, strengthening the view that axis structure controls COs, and the two complexes might control different chromosomal regions.

A Model for the Regulation of CO Sites via Chromosome Structure

Meiotic chromosomes have a highly ordered structure during DSB formation and crossing over. The bivalent appears as a lampbrush, with DNA loops as bristles and the axis as the stem (Zickler and Kleckner, 1999). Loop size and axis length covary. For example, mice defective in *Smc1β,* a subunit of a meiosis-specific cohesin, show an increased DNA loop size and a decreased axis length (Novak et al., 2008). Work in yeast suggests that DSBs occur in DNA loops distal to DNA-axis attachment sites (Blat and Kleckner, 1999; Gerton et al., 2000). Integrating these studies, we speculate that the increase in axis length in condensin-defective animals may reflect a change in loop size and number, which consequently alters DSB and CO distribution. In our experiments, changes in chromosome structure always correlate with dramatic changes in the distribution of DSBs and COs, regardless of whether their number increases. We propose that condensin controls chromosome structure and distribution of axial attachment points, which then dictate the density and position of DNA loops, and hence DSBs.

EXPERIMENTAL PROCEDURES

CO Analysis

Crossover analysis was conducted as in Tsai et al. (2008). SNP markers for chromosome III are listed in Table S2. In cases where γ-irradiation was used, wild-type or mutant animals were mated into the CB4856 Hawaiian variant. One hundred L4 stage hermaphrodite cross progeny were transferred to M9 media in a 1.5 ml eppendorf tube and subjected to 2.5, 5, or 7.5 Gy from a sealed ^{137}Cs source. Ten irradiated hermaphrodites were transferred to individual NG agar plates with an OP50 lawn and mated with approximately ten wild-type males. After 12 hr, all animals were transferred to new plates and allowed to lay embryos for 24 hr. Males arising from embryos laid during this interval were then assayed individually for crossover events, as in (Tsai et al., 2008).

RNAi

Bacteria containing a vector (MRC Geneservice) for isopropyl-β-D-thiogalactopyranoside (IPTG)-inducible expression of double stranded RNA coding for *ced-4* (open reading frame [ORF]: C35d10.9), *rad-54* (ORF: W06D4.6), or *unc-22* (ORF: ZK617.1) were grown overnight at 37°C in Luria broth containing 50 μg/ml ampicillin. After ~12 hr, IPTG was added to a final concentration of 4 mM. After 2 hr further growth, cultures were harvested and plated on NGM agar containing 1 mM IPTG and 1 μg/ml carbenicillin (Sigma-Aldrich). After 12 hr incubation at 25°C, young adult animals, either wild-type or mutant, were transferred to the plates and allowed to lay embryos for 12 hr at 20°C, after which the parents were removed. Once at L4 stage, progeny were dissected and analyzed cytologically.

RAD-51 Analysis

RAD-51 foci were quantified as in (Tsai et al., 2008). Only fully separated foci were counted as single foci, thus the numbers are likely to be an underestimate. Some animals treated with *rad-54*(RNAi) showed significant apoptosis as scored by DAPI morphology. These germlines were not quantified.

TUNEL Assay

DNA DSBs were detected directly using terminal dioxynucleotidyl transferase to attach fluorescently labeled nucleotides to 3′ DNA ends. In brief, whole-mount *C. elegans* gonads were labeled using an In Situ Cell Death Detection Kit (Fluorescence) (Roche) with incubation in a temperature-controlled microwave. The fluorescene signal was amplified by staining with anti-fluorescein primary antibody (Rockland) followed by fluorescene-conjugated secondary antibody (Roche). Samples were imaged as described for chromosome axis length measurements. Details are in the Supplemental Experimental Procedures.

TUNEL and RAD-51 Costaining

TUNEL and RAD-51 costaining experiments were preformed as for TUNEL alone, with modifications as listed in the Supplemental Experimental Procedures.

Chromosome Axis Length Measurements and RAD-51 Distribution Assays

For axis length measurements and RAD-51 distribution assays, whole-mount *C. elegans* gonads were labeled by FISH, either with two oligonucleotide probes to X or two probes made from fosmids to chromosome I. After FISH, gonads were stained with HTP-3 and RAD-51 antibodies followed by secondary antibodies (Molecular Probes). Images were collected on a confocal microscope and deconvolved with Huygens Pro (Scientific Volume Imaging) software. Chromosomes were traced in 3D along the HTP-3-stained axis and straightened computationally. For each chromosome, axis length and positions of FISH probes and RAD-51 foci were measured. Details are in the Supplemental Experimental Procedures.

SUPPLEMENTAL DATA

Supplemental Data include Supplemental Experimental Procedures, eight figures, and three tables and can be found with this article online at http://www.cell.com/supplemental/S0092-8674(09)00915-5.

ACKNOWLEDGMENTS

We thank S. Uzawa for microscopy advice, A. Gartner for RAD-51 antibody, A. Dernburg for HTP-3 antibody, S. Ruzen for computing facilities, J. Gunther for figure design, and T. Cline, A. Severson, C. Tsai, S. Uzawa, and A. Wood for discussions. D.G.M. was funded by training grants T32GM07127 and T32GM07232. B.J.M. is an investigator of the Howard Hughes Medical Institute.

Received: November 13, 2008
Revised: May 17, 2009
Accepted: July 8, 2009
Published online: September 24, 2009

REFERENCES

Alpi, A., Pasierbek, P., Gartner, A., and Loidl, J. (2003). Genetic and cytological characterization of the recombination protein RAD-51 in *Caenorhabditis elegans*. Chromosoma *112*, 6–16.

Blat, Y., and Kleckner, N. (1999). Cohesins bind to preferential sites along yeast chromosome III, with differential regulation along arms versus the centric region. Cell *98*, 249–259.

Boulton, A., Myers, R.S., and Redfield, R.J. (1997). The hotspot conversion paradox and the evolution of meiotic recombination. Proc. Natl. Acad. Sci. USA *94*, 8058–8063.

Buhler, C., Borde, V., and Lichten, M. (2007). Mapping meiotic single-strand DNA reveals a new landscape of DNA double-strand breaks in *Saccharomyces cerevisiae*. PLoS Biol. *5*, e324.

Chan, R.C., Severson, A.F., and Meyer, B.J. (2004). Condensin restructures chromosomes in preparation for meiotic divisions. J. Cell Biol. *167*, 613–625.

Chen, S.Y., Tsubouchi, T., Rockmill, B., Sandler, J.S., Richards, D.R., Vader, G., Hochwagen, A., Roeder, G.S., and Fung, J.C. (2008). Global analysis of the meiotic crossover landscape. Dev. Cell *15*, 401–415.

Coop, G., and Myers, S.R. (2007). Live hot, die young: transmission distortion in recombination hotspots. PLoS Genet. *3*, e35.

Coop, G., Wen, X., Ober, C., Pritchard, J.K., and Przeworski, M. (2008). High-resolution mapping of crossovers reveals extensive variation in fine-scale recombination patterns among humans. Science *319*, 1395–1398.

Couteau, F., Nabeshima, K., Villeneuve, A., and Zetka, M. (2004). A component of *C. elegans* meiotic chromosome axes at the interface of homolog alignment, synapsis, nuclear reorganization, and recombination. Curr. Biol. *14*, 585–592.

Csankovszki, G., Collette, K., Spahl, K., Carey, J., Snyder, M., Petty, E., Patel, U., Tabuchi, T., Liu, H., McLeod, I., et al. (2009). Three distinct condensin complexes control *C. elegans* chromosome dynamics. Curr. Biol. *19*, 9–19.

de Massy, B., Rocco, V., and Nicolas, A. (1995). The nucleotide mapping of DNA double-strand breaks at the CYS3 initiation site of meiotic recombination in *Saccharomyces cerevisiae*. EMBO J. *14*, 4589–4598.

Dernburg, A.F., McDonald, K., Moulder, G., Barstead, R., Dresser, M., and Villeneuve, A.M. (1998). Meiotic recombination in *C. elegans* initiates by a conserved mechanism and is dispensable for homologous chromosome synapsis. Cell *94*, 387–398.

Gerton, J.L., DeRisi, J., Shroff, R., Lichten, M., Brown, P.O., and Petes, T.D. (2000). Inaugural article: global mapping of meiotic recombination hotspots and coldspots in the yeast *Saccharomyces cerevisiae*. Proc. Natl. Acad. Sci. USA *97*, 11383–11390.

Goodyer, W., Kaitna, S., Couteau, F., Ward, J.D., Boulton, S.J., and Zetka, M. (2008). HTP-3 links DSB formation with homolog pairing and crossing over during *C. elegans* meiosis. Dev. Cell *14*, 263–274.

Greenawalt, D.M., Cui, X., Wu, Y., Lin, Y., Wang, H.Y., Luo, M., Tereshchenko, I.V., Hu, G., Li, J.Y., Chu, Y., et al. (2006). Strong correlation between meiotic crossovers and haplotype structure in a 2.5-Mb region on the long arm of chromosome 21. Genome Res. *16*, 208–214.

Grey, C., Baudat, F., and de Massy, B. (2009). Genome-wide control of the distribution of meiotic recombination. PLoS Biol. *7*, e35.

Hagstrom, K.A., Holmes, V.F., Cozzarelli, N.R., and Meyer, B.J. (2002). *C. elegans* condensin promotes mitotic chromosome architecture, centromere organization, and sister chromatid segregation during mitosis and meiosis. Genes Dev. *16*, 729–742.

Hillers, K.J., and Villeneuve, A.M. (2003). Chromosome-wide control of meiotic crossing over in *C. elegans*. Curr. Biol. *13*, 1641–1647.

Jeffreys, A.J., and Neumann, R. (2002). Reciprocal crossover asymmetry and meiotic drive in a human recombination hot spot. Nat. Genet. *31*, 267–271.

Jeffreys, A.J., Kauppi, L., and Neumann, R. (2001). Intensely punctate meiotic recombination in the class II region of the major histocompatibility complex. Nat. Genet. *29*, 217–222.

Jones, G.H. (1984). The control of chiasma distribution. Symp. Soc. Exp. Biol. *38*, 293–320.

Kauppi, L., Jasin, M., and Keeney, S. (2007). Meiotic crossover hotspots contained in haplotype block boundaries of the mouse genome. Proc. Natl. Acad. Sci. USA *104*, 13396–13401.

Kauppi, L., Jeffreys, A.J., and Keeney, S. (2004). Where the crossovers are: recombination distributions in mammals. Nat. Rev. Genet. *5*, 413–424.

Keeney, S., Giroux, C.N., and Kleckner, N. (1997). Meiosis-specific DNA double-strand breaks are catalyzed by Spo11, a member of a widely conserved protein family. Cell *88*, 375–384.

Losada, A., and Hirano, T. (2005). Dynamic molecular linkers of the genome: the first decade of SMC proteins. Genes Dev. *19*, 1269–1287.

Maloisel, L., and Rossignol, J.L. (1998). Suppression of crossing-over by DNA methylation in *Ascobolus*. Genes Dev. *12*, 1381–1389.

Mancera, E., Bourgon, R., Brozzi, A., Huber, W., and Steinmetz, L.M. (2008). High-resolution mapping of meiotic crossovers and non-crossovers in yeast. Nature *454*, 479–485.

Martin, J.S., Winkelmann, N., Petalcorin, M.I., McIlwraith, M.J., and Boulton, S.J. (2005). RAD-51-dependent and -independent roles of a *Caenorhabditis elegans* BRCA2-related protein during DNA double-strand break repair. Mol. Cell. Biol. *25*, 3127–3139.

Meyer, B.J. (2005). X-chromosome dosage compensation. In WormBook, The *C. elegans* Research Community, ed. 10.1895/wormbook.1.8.1, http://www.wormbook.org.

Moens, P.B., Kolas, N.K., Tarsounas, M., Marcon, E., Cohen, P.E., and Spyropoulos, B. (2002). The time course and chromosomal localization of recombination-related proteins at meiosis in the mouse are compatible with models that can resolve the early DNA-DNA interactions without reciprocal recombination. J. Cell Sci. *115*, 1611–1622.

Nicolas, A., Treco, D., Schultes, N.P., and Szostak, J.W. (1989). An initiation site for meiotic gene conversion in the yeast *Saccharomyces cerevisiae*. Nature *338*, 35–39.

Novak, I., Wang, H., Revenkova, E., Jessberger, R., Scherthan, H., and Hoog, C. (2008). Cohesin Smc1β determines meiotic chromatin axis loop organization. J. Cell Biol. *180*, 83–90.

Ogawa, T., Shinohara, A., Nabetani, A., Ikeya, T., Yu, X., Egelman, E.H., and Ogawa, H. (1993). RecA-like recombination proteins in eukaryotes: functions and structures of *RAD51* genes. Cold Spring Harb. Symp. Quant. Biol. *58*, 567–576.

Ono, T., Losada, A., Hirano, M., Myers, M.P., Neuwald, A.F., and Hirano, T. (2003). Differential contributions of condensin I and condensin II to mitotic chromosome architecture in vertebrate cells. Cell *115*, 109–121.

Padmore, R., Cao, L., and Kleckner, N. (1991). Temporal comparison of recombination and synaptonemal complex formation during meiosis in *S. cerevisiae*. Cell *66*, 1239–1256.

Page, S.L., and Hawley, R.S. (2003). Chromosome choreography: the meiotic ballet. Science *301*, 785–789.

Page, S.L., and Hawley, R.S. (2004). The genetics and molecular biology of the synaptonemal complex. Annu. Rev. Cell Dev. Biol. *20*, 525–558.

Petes, T.D. (2001). Meiotic recombination hot spots and cold spots. Nat. Rev. Genet. *2*, 360–369.

Shinohara, M., Gasior, S.L., Bishop, D.K., and Shinohara, A. (2000). Tid1/Rdh54 promotes colocalization of Rad51 and Dmc1 during meiotic recombination. Proc. Natl. Acad. Sci. USA *97*, 10814–10819.

Sturtevant, A.H. (1913). The linear arrangement of six-sex linked factors in *Drosophila*, as shown by their mode of association. J. Exp. Zool. *14*, 43–59.

Tsai, C.J., Mets, D.G., Albrecht, M.R., Nix, P., Chan, A., and Meyer, B.J. (2008). Meiotic crossover number and distribution are regulated by a dosage compensation protein that resembles a condensin subunit. Genes Dev. *22*, 194–211.

Villeneuve, A.M. (1994). A *cis*-acting locus that promotes crossing over between X chromosomes in *Caenorhabditis elegans*. Genetics *136*, 887–902.

Winckler, W., Myers, S.R., Richter, D.J., Onofrio, R.C., McDonald, G.J., Bontrop, R.E., McVean, G.A., Gabriel, S.B., Reich, D., Donnelly, P., et al. (2005). Comparison of fine-scale recombination rates in humans and chimpanzees. Science *308*, 107–111.

Xu, L., and Kleckner, N. (1995). Sequence non-specific double-strand breaks and interhomolog interactions prior to double-strand break formation at a meiotic recombination hot spot in yeast. EMBO J. *14*, 5115–5128.

Yauk, C.L., Bois, P.R., and Jeffreys, A.J. (2003). High-resolution sperm typing of meiotic recombination in the mouse MHC Eβ gene. EMBO J. *22*, 1389–1397.

Zickler, D., and Kleckner, N. (1999). Meiotic chromosomes: integrating structure and function. Annu. Rev. Genet. *33*, 603–754.